HIGH-β CAVITY DESIGN – A TUTORIAL*

Sergey Belomestnykh# and Valery Shemelin
Laboratory for Elementary-Particle Physics, Cornell University, Ithaca, NY 14853

Solutions to problems are easy to find:
the problem's a great contribution.
What's truly an art is to wring from your mind
a problem to fit a solution.

Last Things First
P. Hein

Abstract

In this tutorial we describe design principles for high-β superconducting accelerating cavities. Both RF and mechanical aspects of the cavity design are presented. We discuss approaches to cavity shape optimization and illustrate these approaches with computer simulations.

SUPERCONDUCTING CAVITIES FOR HIGH-β ACCELERATORS

A particle accelerator consists of many systems that make the acceleration possible: a particle source, a vacuum chamber, a focusing system and many others. The device that immediately provides the acceleration by imparting energy to the charged particles is usually a microwave resonant cavity. Normal- and superconducting materials are used to fabricate accelerating cavities. As over the last two decades the science and technology of RF superconductivity has evolved and matured [1], more and more modern accelerators began using superconducting (SC) accelerating structures, which have several attractive features as compared to normal-conducting cavities. The most salient of those features are high accelerating field, E_{acc}, in continuous wave (CW) and long pulse operating modes and high quality factor Q_0, a universal figure of merit characterizing the ratio of the energy stored in the cavity to the energy lost in one RF period.

The evolution of superconducting accelerating structures for acceleration of particles with $\beta \approx 1$ (these are light particles, electrons and positrons, or high-energy protons; $\beta = v/c$, where v is the speed of the particle and c is the speed of light) led to cavities with an elliptical cell shape. The length of the cavity gap is usually $L = \beta\lambda/2$, λ being the wavelength, for the so called π mode in multicell cavities. Heavier particles, e.g., ions or low-energy protons, have low values of β. SC cavities for these particles are of different designs: split-ring resonators, half-wave-long and quarter-wave-long coaxial resonators, spoke cavities. The transition between low-velocity cavity shapes and elliptical cavities usually occurs at $\beta = 0.6\ldots0.8$. This is because cavities with elliptical cells for small β become very big as lower frequencies are used and less stable mechanically (the accelerating gap shortens and cavity walls become more vertical). Low-β SC cavity design is discussed in another tutorial [2]. Here we will talk about elliptical cavities for velocity-of-light particles.

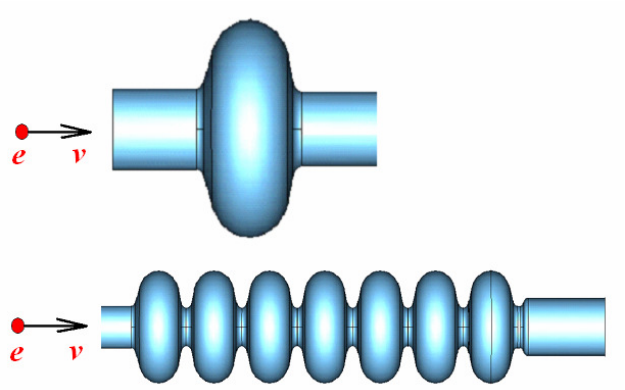

Figure 1: Single cell and multicell elliptical cavities.

The term "elliptical cavity" means that the profile line of the cavity consists of several (usually two) elliptic arcs and, possibly, a straight lines between them. An equatorial arc serves two purposes. Firstly, it was found [3] that this shape eliminates multipacting, which was limiting performance of cylindrical pill-box cavities. Later on [4] it was understood that using an arc of optimal shape in elliptical cavities makes distribution of the magnetic field along the surface more uniform and thus reduces the peak value of the magnetic field in elliptical cavities. This in turn leads to higher accelerating gradients and lower losses. Use of elliptic arcs in the cavity iris area reduces the peak surface electric field [5], which alleviates field emission.

A typical accelerating structure consists of a chain of cells coupled together via irises (Fig. 1). An extreme case is a single cell cavity that is quite often employed in high-current circular accelerators. The beam tubes attached to the end cells allow particles to pass through the structure. Additional ports on the beam tubes serve to bring RF power into the cavity to establish the field and to deliver power to the beam, to sample the cavity field for regulation and monitoring, to extract power of higher-order modes (HOMs) excited by the beam.

The number of cavities in an accelerator can vary from only a few cavities to many thousands. For example, electron-positron storage ring CESR operates with only four single cell superconducting RF cavities [6] (Fig. 5a), while the International Linear Collider (ILC) [7], now under design, will require more than 15,000 accelerating structures, each about one meter long (Fig. 2).

While the main purpose of accelerating cavities is to provide energy to charged particle beams at a fast acceleration rate, operating cavities with the highest

*Supported by the National Science Foundation
#sab@lepp.cornell.edu

achievable gradient is not always optimal for an accelerator. There are machine-dependent and technology-dependent factors that determine operating gradient of RF cavities and influence the cavity design, such as accelerator cost optimization, maximum power through an input coupler, necessity to extract HOM power, etc. Based on accelerating gradient, RF power and HOM damping requirements, one can divide SC cavities into five types listed in Table 1. Figs. 2 through 5 show pictures of different superconducting cavity types. Niobium being the material of choice for SC accelerating cavities, all shown cavities are fabricated out of bulk sheet niobium with the exception of LHC cavity (Fig. 5c), where a thin film of niobium is sputtered on to a cavity fabricated out of copper sheets.

Table 1: High-β cavity types.

	Example	Accelerating gradient	RF power	HOM damping
Pulsed linacs	ILC [7], XFEL[8], Fig. 2	High ($\geq$ 25 MV/m)	High peak (> 250 kW), low average (~ 5 kW)	Moderate ($Q = 10^4 \ldots 10^6$)
CW low-current linacs	CEBAF [9], Fig3; ELBE [10]	Moderate to low (8…20 MV/m)	Low average (5…15 kW)	Relaxed
CW high-current ERLs	Cornell ERL [11], Electron cooler for RHIC [12]	Moderate (15…20 MV/m)	Low average (few kW)	Strong ($Q = 10^2 \ldots 10^4$)
CW high-current injectors for ERLs	Cornell ERL injector [13], Fig.4; JLab FEL 100 mA injector [14]	Moderate to low (5…15 MV/m)	High average (50…500 kW)	Strong ($Q = 10^2 \ldots 10^4$)
CW high-current storage rings	CESR [6], KEKB [15], LHC [16], Fig. 5	Low (5…10 MV/m)	High average (up to 400 kW)	Strong ($Q \sim 10^2$)

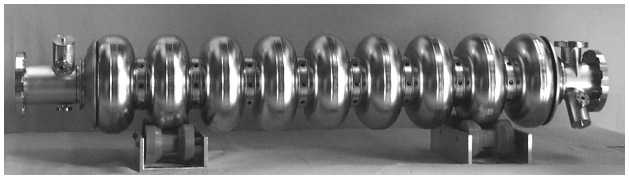

Figure 2: A 1.3 GHz, 9-cell TESLA cavity [17] for ILC and XFEL.

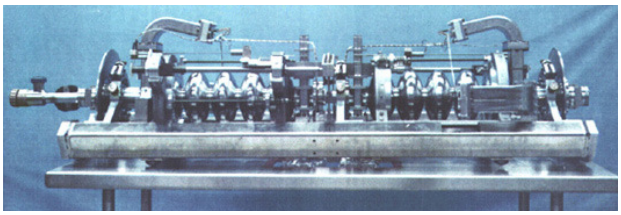

Figure 3: A pair of 1.5 GHz, 5-cell cavities for CEBAF.

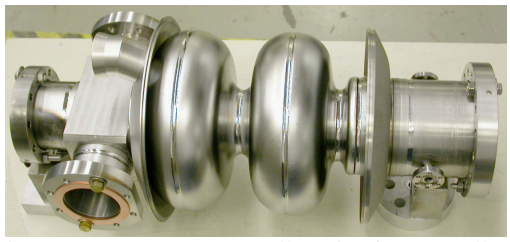

Figure 4: A 1.3 GHz, 2-cell cavity for Cornell ERL injector.

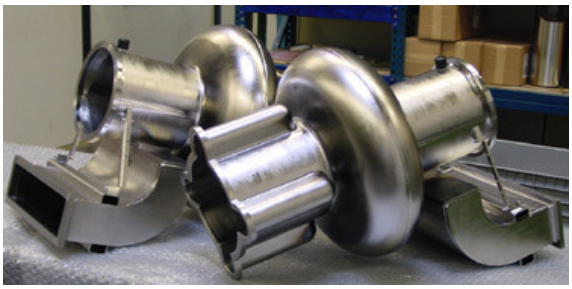

(a)

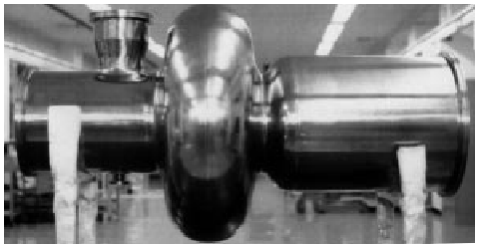

(b)

(c)

Figure 5: Cavities for high-current storage rings. (a) 500 MHz CESR cavities, (b) 508 MHz KEKB cavity, (c) 400 MHz LHC cavity.

FIGURES OF MERIT

Although elliptical cavity shapes are used for the velocity-of-light superconducting cavities, we will often use a single cell pill-box or cylindrical cavity in this section for illustration purposes as one can use analytical formulae for the pill-box cavity without beam pipes. For a very good introduction into resonant cavities we recommend a textbook [18].

An infinite number of eigenmodes having different field distributions and generally different resonant frequencies can exist in a cavity. These modes in the pill-box cavity belong to two families: **transverse magnetic** (TM) modes and **transverse electric** (TE) modes. In some special cases two modes can have the same resonant frequency (degenerate modes). The modes can have different number of variations along each of three cylindrical coordinates (ϕ, r, z) and are designated accordingly. For example, the transverse magnetic mode with one variation along azimuth, two variations along radius and zero variations along longitudinal coordinate z is called TM_{120}. The fundamental, or lowest RF frequency, mode (TM_{010}) is usually employed for particle acceleration as it has the highest shunt impedance (see below).

The cavity is characterized by various parameters (figures of merit). The **operating frequency** f is one of the most important ones. Dimensions of a cavity are of the order of the wave length that is

$$\lambda = c/f \ .$$

On the one hand, using frequencies below several hundreds of megahertz renders the cavity very big and expensive. On the other hand, one cannot use frequencies higher than several gigahertzes because it is hard to fabricate very small cavities and one would need a large number of cavities for a substantial acceleration. Superconducting cavities, as opposed to normal conducting ones, tend to favor lower frequencies, because RF losses in superconductors increase as frequency squared (see description of the surface resistance below).

As can be seen from Fig. 6, for maximal acceleration we need

$$T_{cav} = \frac{d}{\beta c} = \frac{T_{\mathrm{RF}}}{2},$$

so that the field always points in the same direction while particles traverse the cavity. Here T_{cav} is the time interval when a particle, or a bunch of particles, passes through the cavity, d is the length of the cavity and T_{RF} is the period of the radio frequency.

Then the **accelerating voltage** in the cavity is

$$V_{cav} = \left| \int_0^d E_z(r=0,z) e^{ikz} dz \right| = dE_0 T \ ,$$

here E_z is the z component of the cavity electric field, $k = \omega/\beta c$ is the wave number, ω is the angular frequency, E_0 is the electric field amplitude and T is the

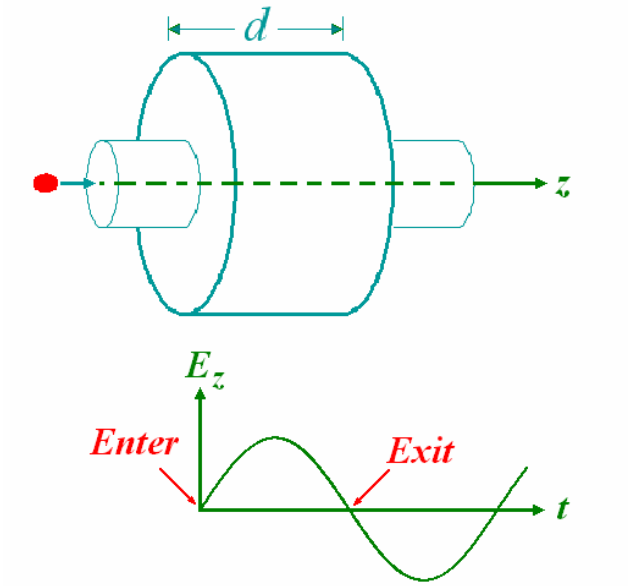

Figure 6: Pill-box cavity with beam tubes and the plot of the cavity electric field vs. time.

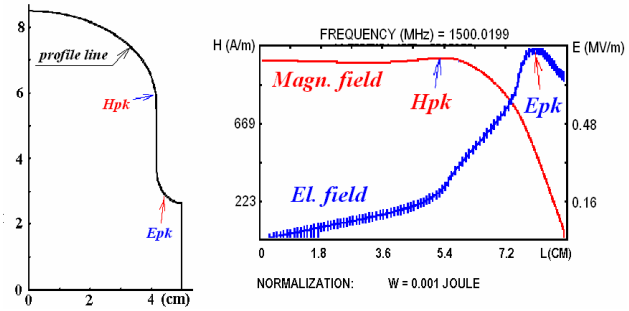

Figure 7: Geometry of an inner half-cell of a multicell cavity and field distribution along the profile line.

transit time factor, which for the pill-box cavity without beam pipes is

$$T = \frac{\sin(kd/2)}{kd/2} = 2/\pi \ , \ \text{for} \ \ d = \lambda/2.$$

The **accelerating field** is $E_{acc} = V_{cav}/d = E_0 T$.

Other important parameters are the maximal, or **peak**, values of the **electric** and **magnetic fields** on the surface**,** E_{pk} and H_{pk}. High surface fields can harm the cavity operation. High surface electric field might cause an electric breakdown and/or field emission in the cavity, which leads to high levels of X-ray radiation and increases the cavity losses. High surface magnetic field might cause a quench or thermal breakdown in a superconducting cavity. More details on the detrimental effects of high surface fields can be found in [1]. Fig. 7 shows fields along the cell profile line and the locations of peak surface fields for an inner half-cell of a multicell cavity.

Peak fields are proportional to the accelerating field in the cavity, thus the values E_{pk}/E_{acc} and H_{pk}/E_{acc} do not depend on the accelerating voltage and are called **normalized electric** and **magnetic fields**. The normalized fields depend only on the shape of the cavity. Typical

values of E_{pk}/E_{acc} are 2…2.6; typical values of H_{pk}/E_{acc} are 40…50 Oe/(MV/m).

For RF currents superconducting materials are not loss-free even at temperatures close to 0 K. The very small, compared to normal conducting materials, losses are characterized by the RF **surface resistance** R_s, which can be expressed as

$$R_s = A(1/T) f^2 e^{-\frac{\Delta(T)}{kT}} + R_0.$$

Here A is a material-dependent constant, 2Δ is the energy gap of the superconductor, R_0 is the residual resistance. Typical surface resistance of a well prepared niobium superconducting surface is several tens of nanoohms, while for very good normal conductors the value is in the milliohm range.

Dissipated power, stored energy and the **quality factor** are important figures of merit. The surface current in the cavity is proportional to the magnetic field H. The power dissipated per unit area is

$$\frac{dP_c}{ds} = \frac{1}{2} R_s |\mathbf{H}|^2 .$$

The total power dissipated in the cavity wall is given by the surface integral:

$$P_c = \frac{1}{2} R_s \int_S |\mathbf{H}|^2 \, ds .$$

The stored energy can be calculated as

$$U = \frac{1}{2}\mu_0 \int_V |\mathbf{H}|^2 \, dv = \frac{1}{2}\varepsilon_0 \int_V |\mathbf{E}|^2 \, dv ,$$

since the time averaged energy in the electric field equals that in the magnetic field.

The quality factor of the cavity is defined as

$$Q_0 = \frac{\omega_0 U}{P_c} = 2\pi \frac{U}{T_{RF} P_c} ,$$

which is 2π the number of cycles it takes to dissipate the energy stored in the cavity. A typical value of Q for a normal conducting copper cavity is of the order of $Q_{nc} = 10^4$. A superconducting cavity can have the quality factor of about $Q_{sc} = 10^{10}$.

From the formulae for U and P_c we can derive

$$Q_0 = \frac{\omega_0 \mu_0 \int_V |\mathbf{H}|^2 \, dv}{R_s \int_S |\mathbf{H}|^2 \, ds} .$$

This formula can be re-written as $Q_0 = G/R_s$, where

$$G = \frac{\omega_0 \mu_0 \int_V |\mathbf{H}|^2 \, dv}{\int_S |\mathbf{H}|^2 \, ds} .$$

G is known as the **geometry factor**. From the last equation one can see that it depends on the cavity shape only, not its size.

The **shunt impedance** R_{sh} determines how much acceleration one gets for a given dissipation:

$$R_{sh} = V_{cav}^2 / P_c ,$$

so to maximize acceleration for given P_c one must maximize the shunt impedance.

Another important figure of merit is

$$R_{sh}/Q_0 = V_c^2 / \omega_0 U .$$

This value has not acquired a stable name and is often referred to as **specific shunt impedance** or simply "R over Q". However, some authors call it **geometric shunt impedance,** because it depends only on the cavity geometry similarly to the geometry factor G.

A cavity can be exited at different frequencies corresponding to different modes of oscillations, not only at the fundamental frequency ω_0. Higher-order modes can be exited by the bunched beam passing through the cavity. The higher the beam current is, the more power can be transferred to the fields of HOMs. These parasitic modes can destroy the bunch. The parameter R/Q can be calculated for these modes as well and is used to determine the level of HOM excitation by the charges traversing the cavity.

MULTICELL CAVITY MODES

A multicell cavity can be represented as a system of coupled oscillators. This means that, likewise connected mechanical pendulums, the system can oscillate at different modes with different frequencies. In Fig. 8 one can see two mechanical pendulums connected with a weak spring. This spring does not disturb oscillations when pendulums are swinging "in-phase". However, when they are moving in opposite directions (assuming that they do not collide), the frequency will be slightly higher due to the presence of the spring. The same effect exists in a two-cell cavity: fields in adjacent cells can have the same or opposite directions. These modes are called 0 mode and π mode, corresponding to the phase shift between fields in neighboring cells. Difference in frequencies of two modes is larger if the coupling (the spring) between two cells (pendulums) is stronger. The cell-to-cell coupling is characterized via the coupling coefficient:

$$k_c = 2 \cdot \frac{f_\pi - f_0}{f_\pi + f_0} \cdot 100\% .$$

In a 9-cell cavity we will find nine modes of oscillation forming a fundamental mode **passband**. Plotting frequencies of these modes on a graph (Fig. 9) versus the mode number, we obtain a cosine-like **dispersion curve**, where the 9th point corresponds to the π mode, usually the working mode for superconducting structures. If the frequency of this mode is too close to the frequency of the neighboring mode, the neighboring mode can also be excited by an RF generator. This may be avoided by increasing the aperture cell-to-cell coupling. Higher order modes also form passbands, see for example a detailed study of the TESLA cavity passbands in [19].

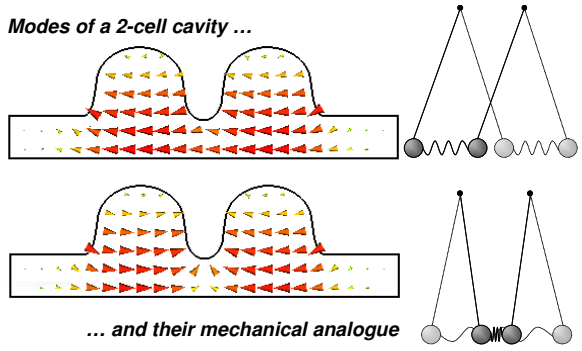

Figure 8: Analogy between a two-cell cavity and two spring-coupled mechanical pendulums.

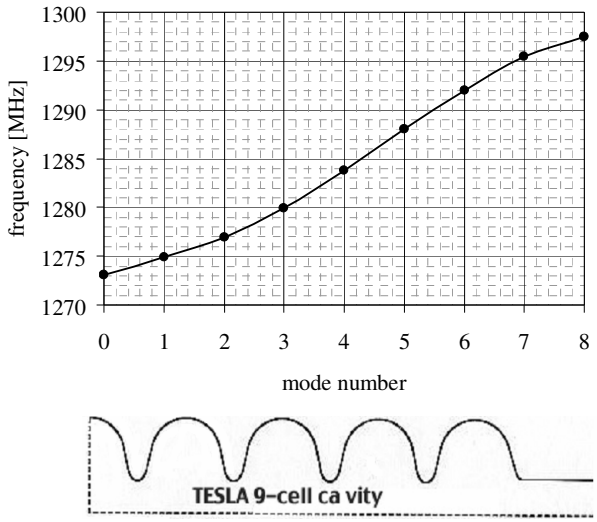

Figure 9: Dispersion curve of the 9-cell TESLA cavity and the cavity geometry. Only one half of the cavity geometry is shown.

USING RF CODES

There are a number of computer programs designed to solve an eigenvalue problem for accelerating cavities. Some codes are designed to solve it for axially symmetric geometries (2-D codes), others can calculate full 3-D problems. Among 2-D codes we would like to mention SUPERFISH [20], and SuperLANS [21]. 3-D codes such as MAFIA [22], Microwave Studio [23], HFSS [24] and others, are usually less accurate and have larger runtime. For faster calculation it is sometimes convenient to remove elements that break axial symmetry and solve the 2-D problem first; then add asymmetric elements and use a 3-D code to find out how those elements disturb the fields and change the cavity parameters. Below we briefly describe features of several RF codes.

*Example 1: **SuperLANS***

SuperLANS (or **SLANS**) is designed to calculate monopole modes of axially symmetric RF cavities using a finite element method of calculation and a mesh with quadrilateral bi-quadratic elements (Fig. 10).

SLANS calculates the mode frequency and many secondary parameters such as the quality factor, stored energy, transit time factor, geometric shunt impedance, maximal electric and magnetic fields, acceleration, acceleration rate. The program interface allows plotting for a given mode its field distribution along axis, force lines, and surface fields. All fields can be written into output file in ASCI format.

Input data for SLANS present a table (insert in Fig. 10) describing the boundary of a cavity geometry. The boundary may consist of straight segments and elliptic arcs. If the cavity is symmetric, only one half of its geometry may be entered while specifying a boundary condition at the plane of symmetry. This boundary condition can be either “electric wall” or “magnetic wall”. SLANS also allows including lossless dielectric materials into the cavity geometry. There are more codes belonging to the SLANS family. **CLANS** solves eigenvalue problem for monopole modes in geometries containing lossy dielectric and ferromagnetic insertions. Programs **SLANS2** and **CLANS2** calculate azimuthally asymmetric (dipole, quadrupole, etc.) modes in cavities. The latter program allows including lossy materials.

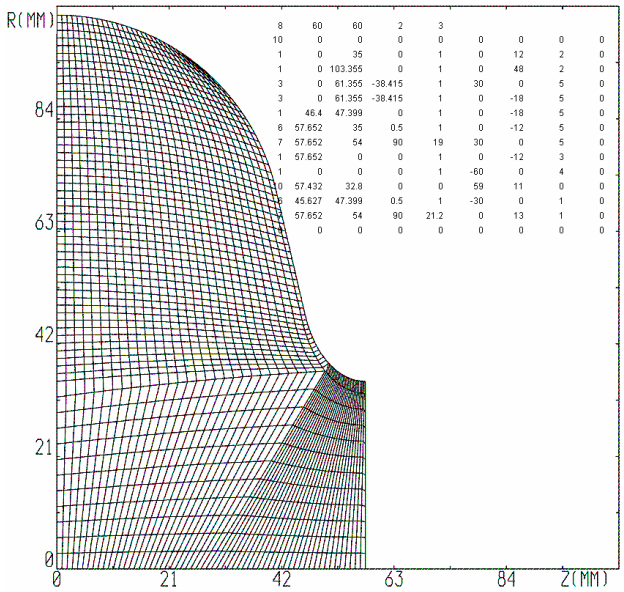

Figure 10: TESLA cell geometry and its description in SLANS.

*Example 2: **MAFIA***

MAFIA is an acronym of **MA**xwell’s equations using the **F**inite **I**ntegration **A**lgorithm. It is a suit of modules that can calculate not only RF cavities, but other electromagnetic structures, including electrostatic and magnetostatic devices. It also includes time domain and particle-in-cell solvers. MAFIA has been quite extensively used in the accelerator physics community. An example of the 3-D model of CESR B-cell cavity for MAFIA is shown in Fig. 11.

Example 3: ***Microwave Studio***

This is relatively recent addition to the field of 3-D RF codes. It combines a user friendly interface and good simulation performance. This code surpasses MAFIA as a more precise tool for RF cavity calculations. Microwave Studio makes the process of inputting the structure geometry more convenient by providing a powerful solid modeling front end. Strong graphic feedback simplifies the definition of the device under investigation even further. After the components have been modeled, a fully automatic meshing procedure is applied before a simulation engine is started. Perfect Boundary Approximation increases accuracy of the simulation by an order of magnitude in comparison to conventional simulators. Since no method works equally well in all application domains, the software contains three different simulation techniques (transient solver, frequency domain, eigenmode solver) to best fit the application. Full parameterization of the structure modeler enables the use of variables in the definition of components. Fig. 12 presents a Microwave Studio model of the Cornell ERL injector SC cavity.

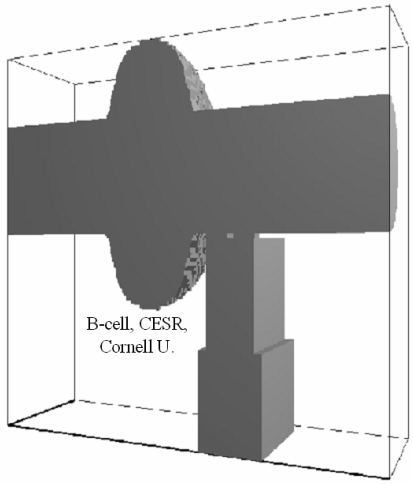

Figure 11: 3-D model of CESR B-cell cavity for MAFIA calculations [25].

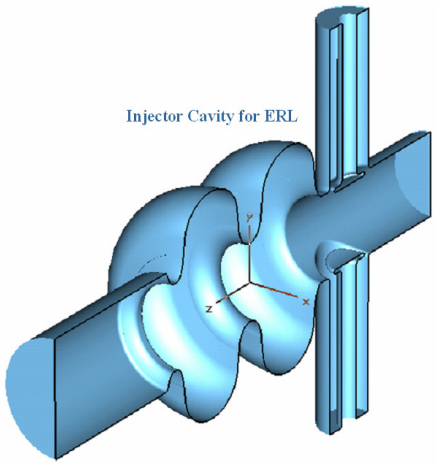

Figure 12: Microwave Studio model of the Cornell ERL injector cavity.

CAVITY DESIGN ISSUES

Although the cavity is the heart, the central part of an accelerating module, it is only one of many parts and its design cannot be easily decoupled from the design of the system as a whole. Very often requirements to different parts of the cryomodule are competing. Fig. 13 illustrates the complex relationship between the accelerator requirements, associated effects, cavity parameters and the cryomodule and cavity design. Below we briefly explain some machine-related design issues.

The radiation pressure due to the cavity electromagnetic field causes a small deformation of the cavity shape resulting in a shift of the cavity resonant frequency, so-called Lorentz-force detuning. This effect can be especially detrimental for a **pulsed operation**, as it causes the cavity frequency change during the RF pulse. Optimizing the cavity shape and employing stiffeners can somewhat alleviate the problem. Further improvement can be obtained by using a fast tuner, piezo-electric or magneto-strictive, to compensate the detuning during the pulse.

Operating superconducting cavities in **CW regime** at moderate to high accelerating gradients leads to a significant RF power dissipation in the cavity walls and hence a significant cryogenic load. The cavity shape optimization aiming to increase the shunt impedance helps to reduce this load. CW operation also influences the operating frequency and temperature choice. Careful thermal analysis of the cryomodule is a must, as the heat flow should be intercepted and carried away and all cryogenic piping should be sized appropriately.

A **high-current bunched beam** passing through a cavity interacts not only with the cavity fundamental mode, being accelerated by its electromagnetic field, but also with the higher-order modes. The latter interaction is undesirable as it can cause various instabilities of beam motion. To reduce the parasitic effect of the beam-HOM interaction, one needs to pay close attention to the properties of HOMs during the cavity shape optimization process and design special HOM absorbers for strong damping of the parasitic modes.

The other aspect of the high-current operation is heavy beam loading of the accelerating structure. The active part of the beam loading is responsible for high RF power demand, while the reactive part should be compensated by appropriate detuning of the cavity (tuner design issue) or can be dealt with by RF control feedback loops, or both.

A **high beam power transfer** requirement limits the choice of operating frequencies as there are very few high-power RF tubes available. It requires cavities to have low external quality factor, which in turn affects the cavity shape optimization and the input coupler design.

The **beam quality** (emittance) should be preserved during machine operation. To assure this, one has to reduce unwanted interaction of the beam with not only HOMs, but also with the transverse components of the fundamental mode electric and magnetic fields by carefully aligning the cavity relative to the beam axis (mechanical design of the cavity and cryostat) and

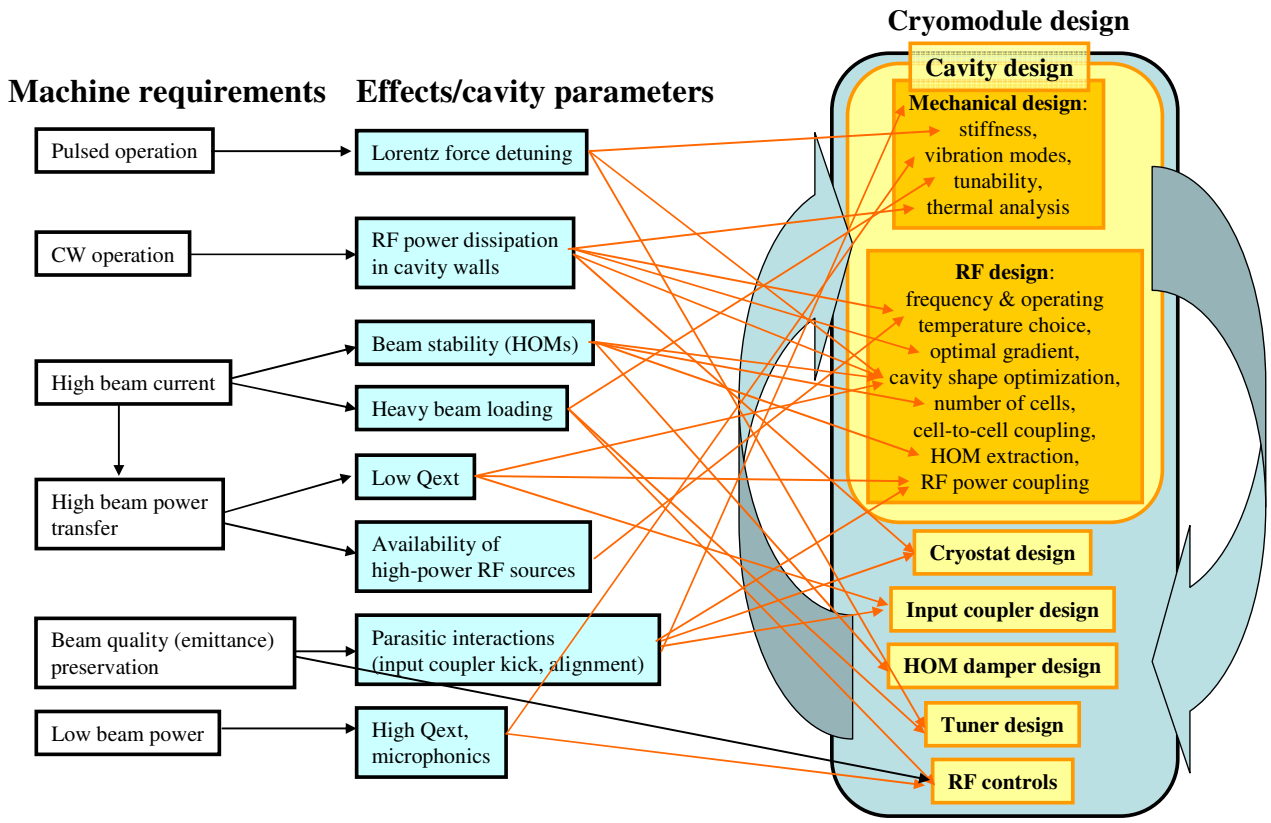

Figure 13: Machine-related cavity design issues.

reducing transverse kick caused by the input coupler and HOM couplers.

If the machine operates with **low beam power**, it is desirable to make external Q factor as high as possible to reduce the RF power from the transmitter. The limiting effect in this case is often the microphonic noise. It can be reduced by careful mechanical design of the cryomodule and use of special feedbacks.

It is obvious that in a short tutorial like this one, it is impossible to thoroughly present all aspects of the cavity design so we will concentrate on some issues, briefly describe others and only mention the rest of them.

CAVITY SHAPE OPTIMIZATION

To minimize the fundamental mode losses (P_c) in the cavity, one must maximize $G \cdot R_{sh}/Q_0$:

$$P_c = \frac{V_{cav}^2}{R_{sh}} = \frac{V_{cav}^2}{Q_0 \cdot (R_{sh}/Q_0)} = \frac{V_{cav}^2}{(R_s \cdot Q_0)\cdot (R_{sh}/Q_0)/R_s} = \frac{V_{cav}^2 \cdot R_s}{G \cdot R_{sh}/Q_0}.$$

The value $G \cdot R_{sh}/Q_0$, similar to both of its components, depends only on the cavity geometry and hence is more convenient for comparing cavities of different designs than the shunt impedance, which depends on material properties and operating frequency. It will be used later in our example of cavity optimization.

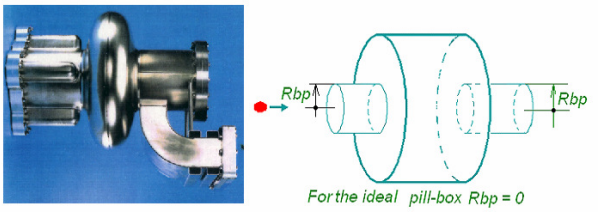

Quantity	CESR B-cell	Ideal pill-box
G	270 Ω	257 Ω
R_{sh}/Q_0	88 Ω	196 Ω
E_{pk}/E_{acc}	2.5	1.6
H_{pk}/E_{acc}	52 Oe/(MV/m)	30.5 Oe/(MV/m)

Figure 14: Comparison of two single cell cavities.

Since cavities are designed for different applications, one has to make different trade-offs in their designs. Compare, for example, values of G and R/Q for two cavities (Fig. 14): the CESR superconducting B-cell cavity and the pill-box cavity without beam pipes. The beam current in CESR is high, which necessitated making beam pipes large to allow propagation of HOMs. It resulted in the increase of H_{pk} and E_{pk} and in a drop of R/Q. This illustrates the trade-off when the performance of the fundamental mode was somewhat compromised to

improve characteristics of higher-order modes for the high beam current operation of CESR.

EXAMPLE OF *G×R/Q* OPTIMIZATION: LOW LOSS CAVITY

A new cavity shape, optimized for low losses (LL shape, Fig. 15), was proposed in [26] for the CEBAF 12 GeV upgrade. The original data and our calculations with SLANS are presented in Table 2. Although there are some discrepancies in results (within +2…-1%), we consider them small. We will use this geometry as a reference and are going to show below how our optimization procedure produces similar geometry.

Table 2: Low Loss cavity parameters.

	Original data [26]	**SLANS results**
E_{pk}/E_{acc}	2.17	2.21
H_{pk}/E_{acc}	37.4 Oe/(MV/m)	37.6 Oe/(MV/m)
kc	1.49 %	1.47 %
R/Q	128.8 Ohm	128.9 Ohm
G	280.3 Ohm	278.2 Ohm
G×R/Q	36,103 Ohm^2	35,848 Ohm^2

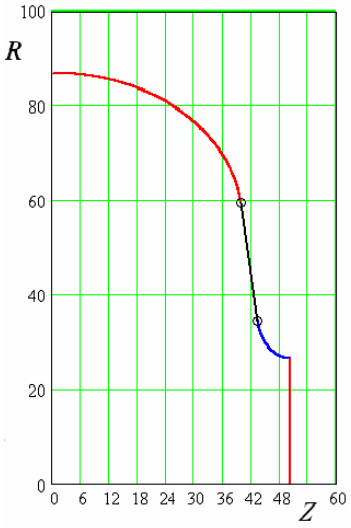

Figure 15: Low loss cavity for JLab's 12 GeV upgrade.

Let us imagine that we do not know the geometry of the optimized cavity. Initially we choose the shape similar to the original Cornell geometry designed for CEBAF with 75-degree tilted wall. The initial shape, Fig. 16, has the following dimensions: $A = B = 34.21$ mm (circular equatorial region), $a = 10$ mm, $b = 20$ mm.

We will search for a shape that has E_{pk}/E_{acc} and H_{pk}/E_{acc} not worse than in the LL cavity, and with maximized $G\times R/Q$. Our initial shape is far from optimized by losses (10.6% higher) and by H_{pk}/E_{acc} (8.4% higher). However E_{pk}/E_{acc} is 11.8 % lower.

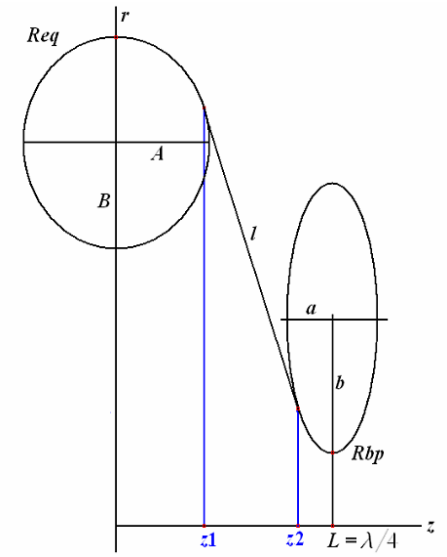

Figure 16: The initial shape.

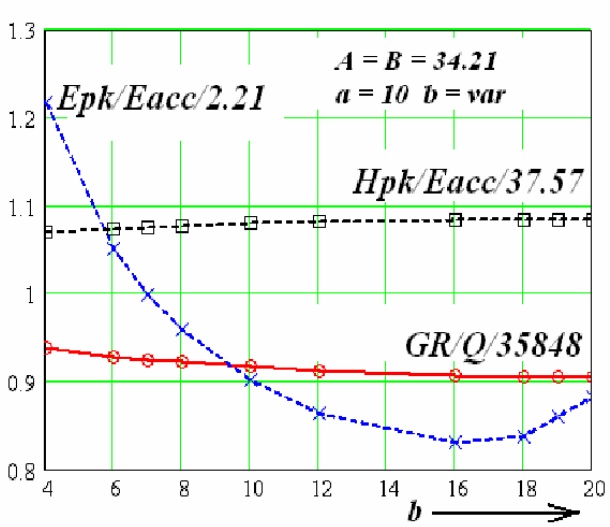

Figure 17: Normalized values as functions of *b*.

There are only four independent parameters that can be used for optimization: *A*, *B*, *a*, and *b*. The half-cell length *L* is predetermined as a quarter of the wave length. The radius of the beam pipe R_{bp} is set by accelerator requirements and is not a subject of this optimization, the equatorial radius R_{eq} will be adjusted by the code to tune the cavity resonant frequency, the length of the straight segment *l* is determined from the condition that it is tangential to the two ellipses.

Let us first see how much progress one can make by changing only one of the geometric parameters, namely *b* (Fig. 17). Here we normalize values of E_{pk}/E_{acc}, H_{pk}/E_{acc}, and $G\times R/Q$ so that for the LL geometry all of them are equal to 1. First we need to decrease normalized H_{pk}/E_{acc} below 1, while keeping normalized E_{pk}/E_{acc} below 1 as well. From Fig. 17 one can see that in this case the best value for *b* is 7 mm (we cannot go further as normalized E_{pk}/E_{acc} reaches 1). However, the improvement in H_{pk} and $G\times R/Q$ is not big (2.1 % for the latter). It is clear that one

needs to vary all four independent parameters in a search for an optimized geometry.

Algorithm of cavity optimization for Low Losses. There are many methods to search for a minimum of a function of many variables. But most of them work poorly with additional restrictions such as normalized fields < 1. Further, changing *A*, *B*, *a*, and *b* separately does not help too much. We propose to use the following algorithm:

1. We check values of $G\times R/Q$ and other relevant parameters making steps in all 4 coordinates (*A*, *B*, *a*, and *b*), including simultaneous steps. This gives us 80 points, plus the central point. The total number of points (or nodes) for calculations is 81 (Fig. 18).
2. We take the best value of $G\times R/Q$ on this 4-dimensional cube under the condition that normalized E_{pk} and $H_{pk} < 1$ (during initial steps we will decrease normalized H_{pk} to 1).
3. If the goal function $G\times R/Q$ improves when we have 2 steps in a row along the same coordinate, we double the step size for this coordinate. If the goal function along some direction is not improved we halve the step size for this direction.
4. Additionally, some elements of the gradient method are also used.

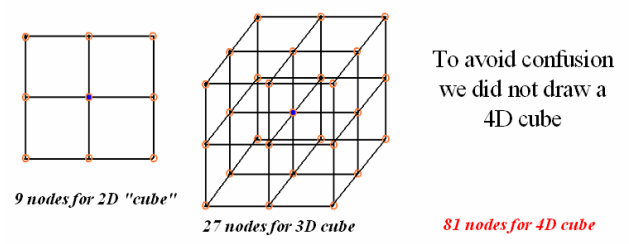

Figure 18: Illustration to the algorithm of optimization.

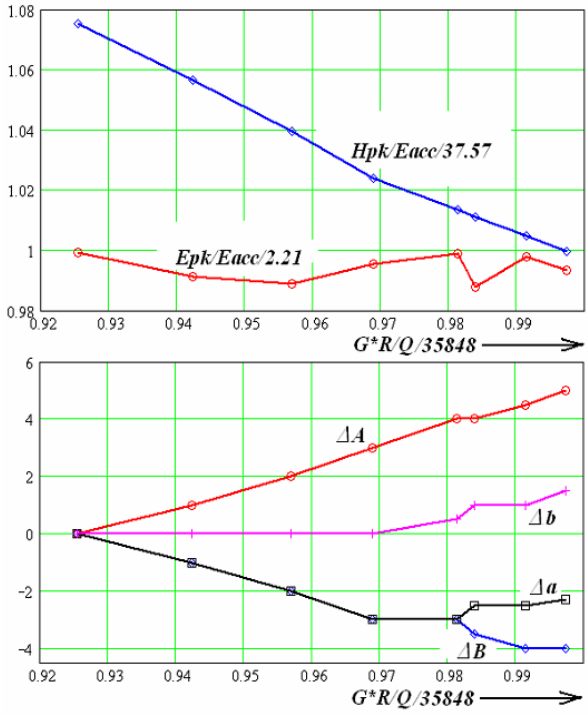

Figure 19: First run: decrease E_{pk} and H_{pk}. Geometrical parameters are in mm.

Following the described algorithm we can reduce the value of normilized H_{pk}/E_{acc} to 1, keeping the normalized E_{pk}/E_{acc} below 1 (Fig. 19, upper graph). Value of $G\times R/Q$ improved because lower H_{pk} means lower losses. The lower graph in Fig. 19 shows the change in geometrical parameters.

Thus we have obtained practically the same results as for the LL cavity, and nearly the same shape. However, one can continue the optimization and improve $G\times R/Q$ even further. An additional 2% can be gained as shown in Fig. 20.

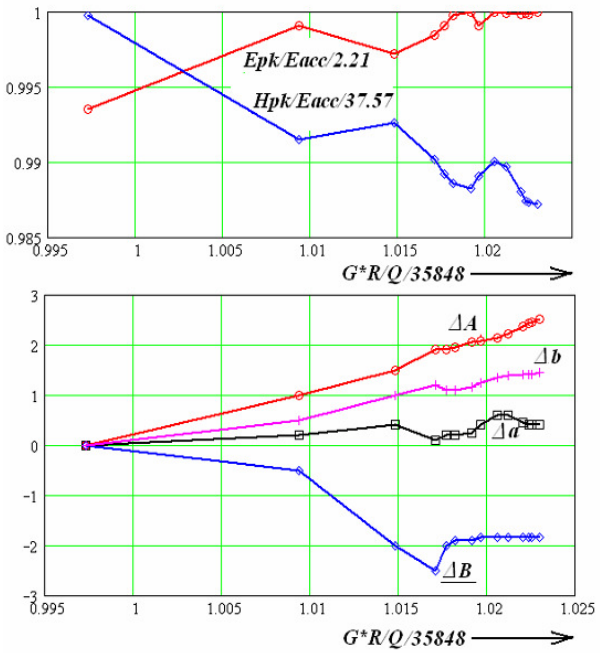

Figure 20: Second run: further improvement of $G\times R/Q$.

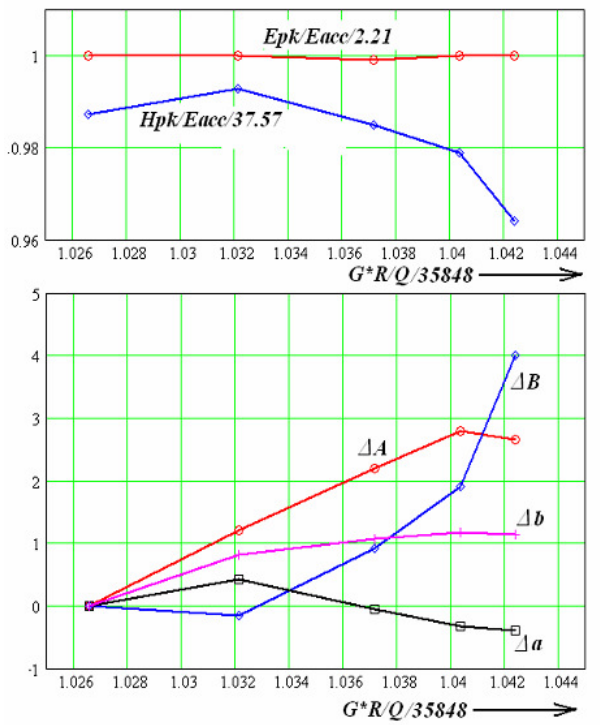

Figure 21: Third run: let's go reentrant.

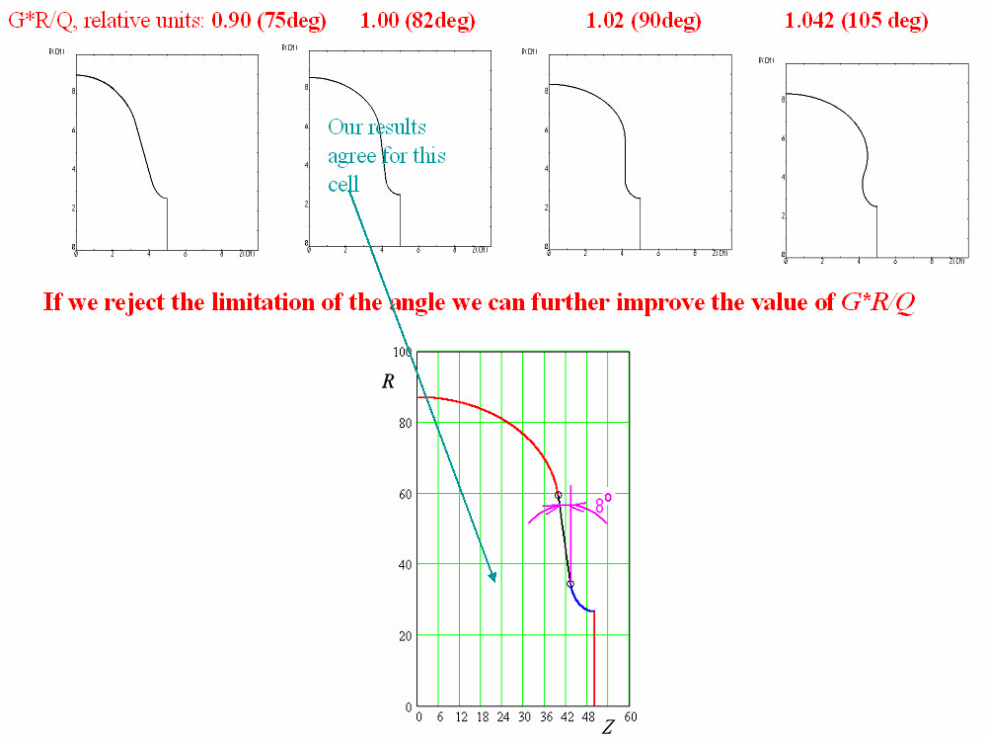

Figure 22: Consecutive change of the shape during optimization for low losses.

Checking the cell shape reveals that the slope of the cavity wall at the point of conjugation of two elliptic arcs becomes 90°. This is likely the reason why the LL cavity was not optimized to this stage: the slope angle of about 82° lets liquid flow easily from the surface during chemical treatment and high pressure rinsing.

There is no, though, fundamental reasons to restrict this angle to be less than 90°. Removing this restriction allows us to continue the optimization. The geometry then becomes reentrant, which gives us an additional 2% improvement in $G \times R/Q$ (Fig. 21).

Fig. 22 illustrates the consecutive change of the shape from the original to the reentrant after each run of the optimization procedure as described above.

The cavity with reentrant shape presents some technological challenges. It is more difficult to perform chemical etching and high pressure rinsing on such geometry. The geometry is also mechanically weaker than the regular non-reentrant cavity. However, it has lower losses and potentially higher accelerating gradient. Recent experiments at Cornell have shown that the technological challenges can be overcome and a very high gradient was obtained with the reentrant shape cavity [27].

MULTIPACTING

Multipacting (MP) is a phenomenon of resonant secondary electron multiplication in RF structures operated under vacuum. It is an undesirable effect that can lead to a build-up of large number of electrons, which absorb RF power so that it becomes impossible to increase the cavity fields by raising the incident power. MP is a common phenomenon in cavities and input couplers. It is very important to do simulations of MP during the cavity design stage. Indeed, multipacting was once a limitation of accelerating gradient in superconducting RF cavities.

Electrons emitted from the RF surface into the cavity follow a trajectory such that they impact back at the surface an even-integer (one point MP, Fig. 23) or odd-integer (two point MP) number of half RF periods after emission. If the secondary emission yield of the surface material is larger than unity, then impacting electrons free more electrons causing an avalanche effect.

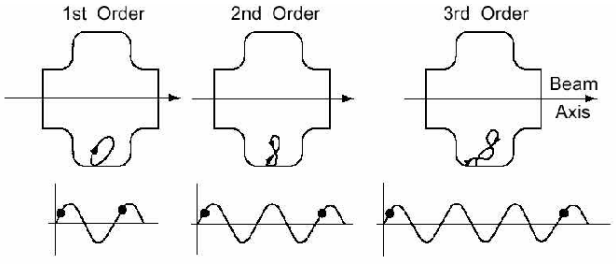

Figure 23: Typical one-point multipacting trajectories of first to third order [1].

It was overcome in superconducting cavities by adopting spherical/elliptical cell shape [3]. In such geometry electrons drift to equatorial region, where electric field is near zero (Fig. 24). As a result MP electrons gain very little energy and MP stops.

However, at high accelerating gradients conditions exist for stable multipacting [28, 29], though it is usually very

weak and easily processed. Fig. 25 shows stable electron trajectories near the cavity equator at peak electric field of 45 MV/m.

Boundaries of the MP zones can be found analytically only for a few special geometries. In all other cases computer codes can be utilized. There are several such codes available, see details in review papers [30, 28].

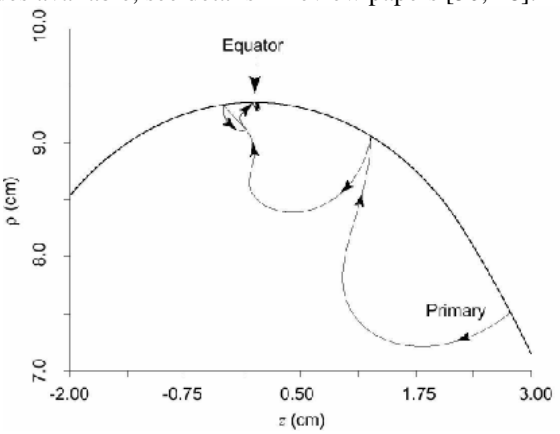

Figure 24: Electron trajectories in an elliptical cavity [1].

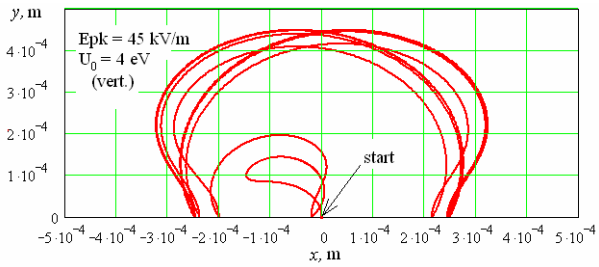

Figure 25: Stable electron trajectories of a two-point MP near the cavity equator.

BEAM-CAVITY INTERACTION

As a bunch of charged particles traverses a cavity, it deposits electromagnetic energy, which is described in terms of wakefields (time domain) or higher-order modes (frequency domain), see Fig. 26. Subsequent bunches are affected by these fields and at high beam intensities one must consider instabilities.

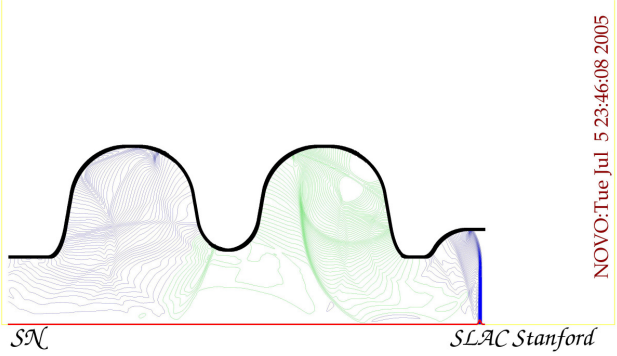

Figure 26: Wakefields of a bunch passing through a two-cell cavity, calculated using computer code NOVO [31].

Fine details of the wakefields themselves are usually of a lesser interest than the integrated effect of a driving charge on a test particle traveling behind it as both particles pass through a structure. The integrated field seen by a test particle traveling on the same path at a constant distance s behind a point charge q is the longitudinal wake (Green) function $w(s)$. Then the wake potential is a convolution of the linear bunch charge density distribution $\lambda(s)$ and the wake function:

$$W(s) = \int_{-\infty}^{s} w(s-s')\lambda(s')ds' .$$

Once the longitudinal wake potential is known, the total energy loss is given by

$$\Delta U = \int_{-\infty}^{\infty} W(s)\lambda(s)ds .$$

The more energy the first bunch looses, the more the likelihood of adverse effects on the subsequent bunches.

Now we can define the loss factor, which tells us how much electromagnetic energy per unit charge a bunch leaves behind in a structure:

$$k = \frac{\Delta U}{q^2} .$$

The following programs are used for calculations in the time domain: **ABCI** [31], **NOVO** [32] (both are 2-D), and **MAFIA** [22] (3-D). The programs cannot calculate Green functions, but only wake potentials for bunches of a finite length.

In the frequency domain fields in the cavity are represented as an infinite sum of fields of its eigenmodes. The lowest, or fundamental mode is usually used for acceleration. The rest of them (HOMs) are responsible for the energy loss and various beam instabilities. The counter-part of the wake potential is the impedance. For a single mode one can calculate the loss factor as

$$k_{\delta n} = \frac{\omega_n}{4}\left(\frac{R}{Q}\right)_n ,$$

and then the longitudinal wake potential as

$$W_n(s) = 2k_{\delta n}\cos\left(\frac{\omega_n s}{c}\right), s > 0 .$$

The total wake potential is an infinite sum of individual mode wake potentials. For mode details on wakefields and wake potentials we refer the readers to an excellent introduction by P. B. Wilson [33].

RF codes (see section “Using RF codes”) can be used to evaluate parameters such as resonant frequency, R/Q and Q of higher-order modes. While these codes work well for modes trapped inside the structure, other methods are employed to calculate parameters of propagating modes.

A time domain (FFT) method is one of the methods to evaluate modes that can propagate inside the beam pipe above cut-off. A long-range wake potential is calculated and then FFT is applied to obtain impedance. The calculation is repeated for longer and longer range until the Q factor of a mode of interest stops changing [34]. This and other methods are discussed in [35].

Why do we need to take special care of HOMs? If they do not decay sufficiently between bunches, then fields from the subsequent bunches can interfere constructively (resonant effect) and cause various instabilities. For example, multi-bunch instabilities in synchrotrons and storage rings or beam break-up instabilities in re-circulating linacs. The growth rate of instabilities is proportional to the impedance of HOMs. This may be especially bad in superconducting cavities, where natural decay of the modes is very weak. That is why practically all SRF cavities have special devices to damp HOMs by absorbing their energy. As these dampers are located on a beam pipe outside the accelerating cell, very often it is necessary to optimize the cavity shape to improve coupling of especially dangerous modes to the damper.

HOM EXTRACTION/DAMPING

The HOM dampers consist of a transmission line attached to the cavity beam pipe via a coupling interface and a broadband terminating load [36]. As most modern accelerators demand strong HOM damping, we will briefly discuss various options. These options include using multiple coaxial antenna/loop couplers (example: TESLA cavity loop coupler [17], Fig. 27), rectangular waveguide dampers [35] (Fig. 28), radial line dampers [37] (Fig. 29), enlarged round (KEKB, Fig. 5b) and fluted (CESR, Fig. 5a) beam pipes, coaxial beam-pipes. The waveguide and beam pipe methods employ transmission lines with cut-off frequency above the cavity fundamental mode frequency thus effectively rejecting it. The other methods require designing a special choke joint or a notch filter for the fundamental mode rejection, which must be carefully tuned prior to installation. As it was already mentioned above, in all cases the transmission line must be terminated by a broadband load. In the case of a widely accepted enlarged beam pipe approach, a section of the beam pipe lined with a microwave absorbing material serves as such load. HOM couplers of this type (Fig. 30) are especially suitable for high-current, short bunch accelerators (KEKB, CESR, Cornell ERL, Electron cooler for RHIC, 4GLS, etc.)

INPUT COUPLER INTERFACE

Both rectangular waveguide (Fig. 31) and coaxial (Fig. 32) couplers are used. Major advantages and disadvantages of two kinds of input couplers are listed in Table 3 [38]. The cavity/coupler interface determines how strongly an RF feeder line is coupled to the cavity. The design of this interface also affects the magnitude of a parasitic transverse kick received by the beam due to non-zero on-axis transverse electromagnetic fields. Here we just mention some interface issues as fundamental power couplers are covered in a separate tutorial [39].

The geometry of the coupling slot in the beam pipe wall determines the coupling strength for waveguide input couplers. An external quality factor of 2×10^5 is achieved in the CESR B-cell cavity [6] with the slot geometry shown in Fig. 33. If weaker coupling is desired, the geometry of the cavity/coupler interface can be quite different as, for example, $\lambda/2$ stub-on-stub design of the original CEBAF cavities, Fig. 34. However, the fields in

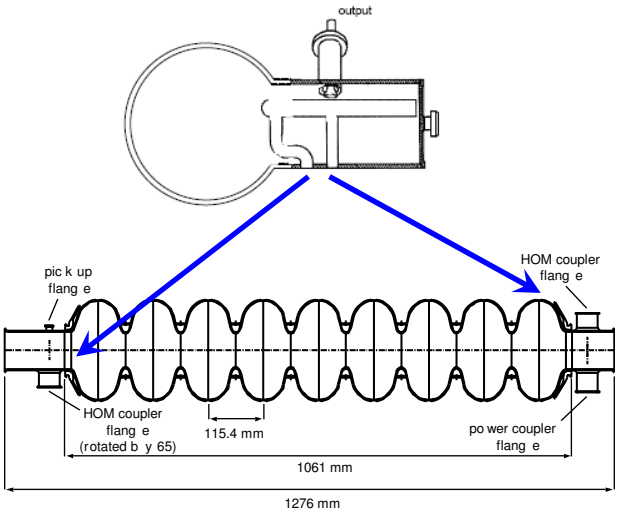

Figure 27: Coaxial loop coupler for superconducting TESLA cavities [17].

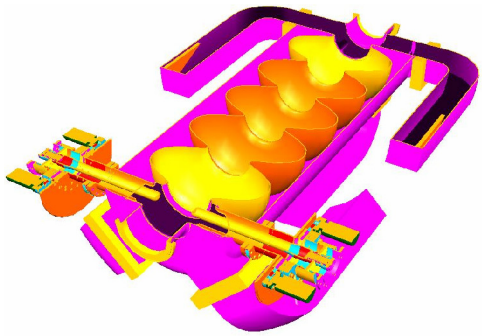

Figure 28: Waveguide HOM dampers [35].

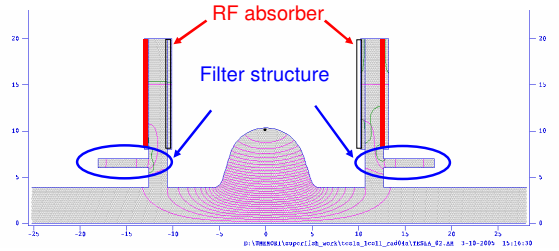

Figure 29: HOM damping using a radial line [37].

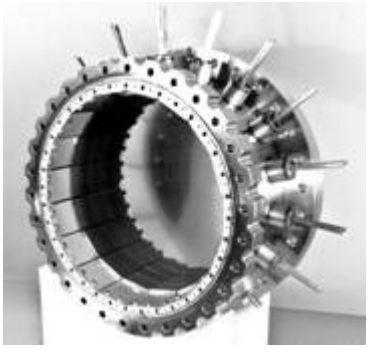

Figure 30: "Porcupine" ferrite-lined beam pipe HOM load of the CESR B-cell cavity [40].

the coupler region are quite asymmetric in this design, producing transverse beam kick. The CEBAF upgrade cryomodule (Fig. 31) is outfitted with an improved design featuring a $\lambda/4$ stub with zero kick to the beam and stronger coupling [41].

In case of coaxial couplers the interface is simply a round port on the cavity beam pipe. The location of this port relative to the cavity and the amount of penetration and the shape of the antenna (the termination of the coaxial line inner conductor) determine the coupling strength. It is easier to make this type of couplers adjustable than the waveguide couplers.

Table 3: Pros and cons of waveguide and coaxial couplers.

	Pros	Cons
Waveguide	• Simpler design • Better power handling • Easier to cool • Higher pumping speed	• Larger size • Bigger heat leak • More difficult to make variable
Coaxial	• More compact • Smaller heat leak • Easier to make variable • Easy to modify multipacting power levels	• More complicated design • Worse power handling • More difficult to cool • Lower pumping speed

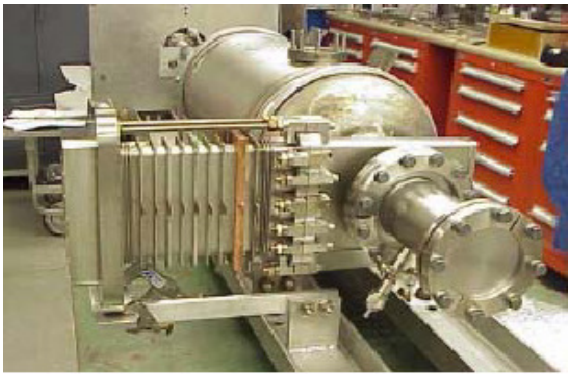

Figure 31: Waveguide coupler for CEBAF upgrade cryomodule [42].

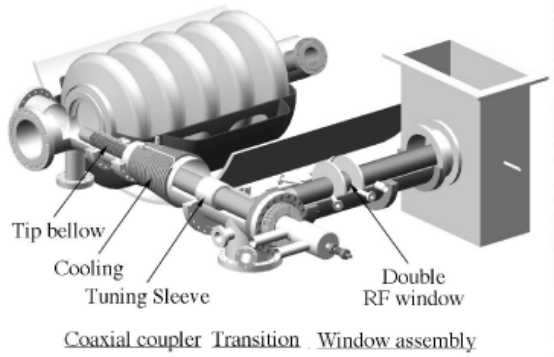

Figure 32: Coaxial coupler for APT cavity [43].

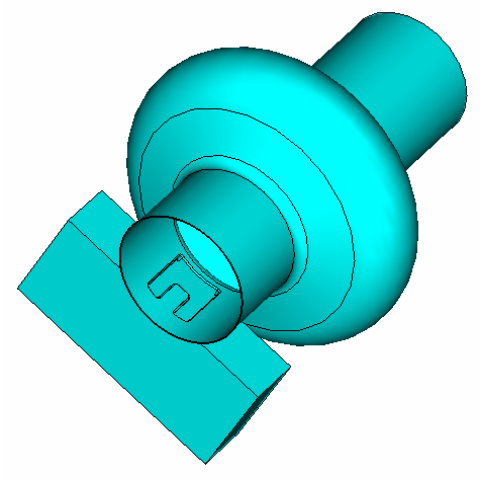

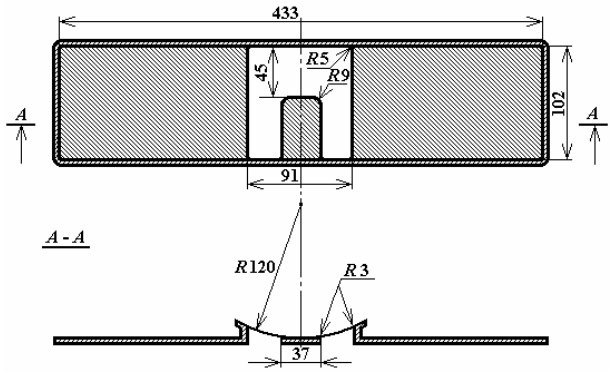

Figure 33: Coupling slot of the CESR B-cell cavity fundamental input coupler [25].

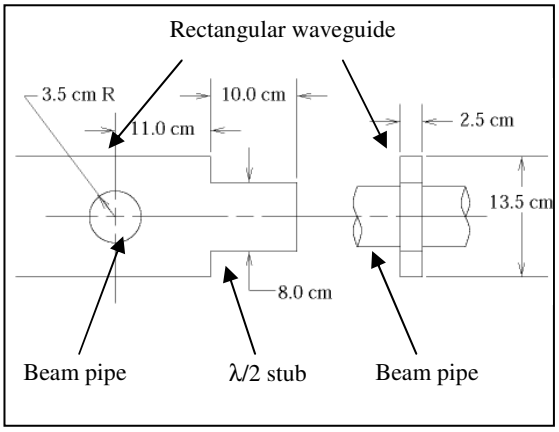

Figure 34: The cavity/coupler interface of the original CEBAF cavities [9].

MECHANICAL ASPECTS OF THE CAVITY DESIGN

A superconducting cavity has to withstand mechanical stresses induced by i) a differential pressure between beam pipe vacuum and atmospheric or sub-atmospheric pressure in the helium vessel, ii) cool-down from room temperature to cryogenic temperatures, iii) tuner mechanism operation, etc. To avoid plastic deformation of cavity walls the cumulative mechanical stress must not exceed the cavity material yield strength. This may

require increase of the cavity wall thickness. On the other hand, very thick walls can compromise heat removal from the inner cavity surface and increase parasitic heat leak from warmer parts of the cryomodule. Careful mechanical and thermal computer simulations are usually performed to assess these issues and find a compromise. Codes like ANSYS [44] are widely used for such simulations. Fig. 35 shows mechanical stress calculation results by ANSYS for CESR B-cell cavity.

The other aspect that affects the choice of the cavity wall thickness is tunability versus Lorentz-force detuning. The electromagnetic field in an RF cavity exerts a pressure on the cavity wall. This radiation pressure causes a small deformation of the cavity walls and a change ΔV of its volume [45]. The net deformation is bending inwards at the cavity iris and outwards at the equator with the consequence of the cavity resonant frequency shift depending on the field amplitude:

$$\frac{\Delta\omega}{\omega} = \frac{1}{4U}\int_{\Delta V}\left(\varepsilon_0 E^2 - \mu_0 H^2\right)dV \ .$$

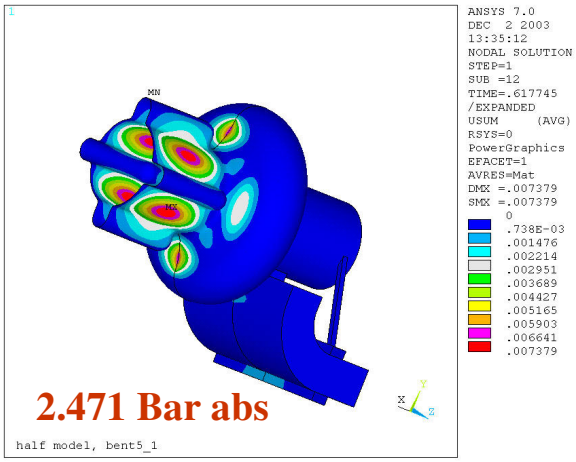

Figure 35: ANSYS simulation of the B-cell cavity. (Courtesy of G.H. Luo, NSRRC.)

The Lorentz-force detuning can be evaluated using a combination of mechanical (e.g., ANSYS) and RF (e.g., Microwave Studio) codes. While in CW operation at a constant field it results in a static detuning easily compensated by the tuner feedback, it may nevertheless cause problems during start-up. It is especially detrimental in pulsed operation, where the dynamics of the detuning plays an important role. Increasing mechanical stiffness of the cavity, for example by stabilizing iris region with stiffening rings [17] somewhat alleviates the problem. Using feedforward techniques can further improve the field stability [46].

One more aspect of the cavity design is careful study of mechanical modes of the cavity itself and as a part of the cryomodule. Any mechanical vibration outside the cryomodule can couple to the cavity exciting its mechanical resonances. Mechanical vibrations of the cavity walls modulate the cavity resonant frequency, which in turn translates in amplitude and phase modulation of the cavity field. This parasitic modulation is frequently called microphonic noise or simply microphonics. Fig. 36 presents an example of ANSYS simulations of vibration modes for a 7-cell superconducting cavity. For more details on ponderomotive instabilities and microphonics we refer readers to the tutorial [47].

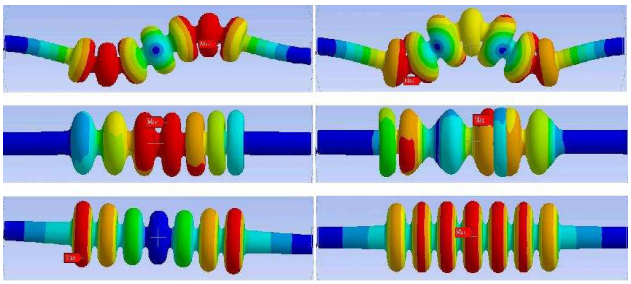

Figure 36: Example of vibration modes of a 7-cell cavity: transverse, longitudinal, breathing (ANSYS simulations). (Courtesy of M. Liepe, Cornell University.)

CAVITY DESIGN EXAMPLE: CORNELL ERL INJECTOR CAVITY

We would like to illustrate how the approaches discussed in this tutorial are applied to a real cavity design. We have chosen the Cornell ERL injector cavity [48] as an example. The superconducting cavities of the injector cryomodule are supposed to provide a total of 500 kW of RF power to a high-average-current beam with the repetition rate of 1300 MHz. Consequently, the permitted beam current depends on the injector energy and varies from 100 mA at 5 MeV to 33 mA at 15 MeV. The acceleration process in the injector must preserve the low emittance of high-brightness beam obtained from the photoemission electron gun. This imposes additional restrictions on the cavity design. Namely the transverse kick from the input coupler has to be minimized and the HOMs have to be damped.

Cavity shape optimization

At an early stage of the project it was decided to limit RF power to 100 kW per input coupler, which determined the need for five cavities. Two reasons determined the number of cells per cavity. On the one hand, the fewer the number of cells the better, as the number of higher-order modes is fewer and it is easier to damp them. On the other hand, one does not want to push the field strength too much as we are already pushing the average RF power per cavity to 100 kW. Thus the trade-off is two cells per cavity, which sets the accelerating gradient in the range from 4.3 to 13 MV/m.

Having the same frequency as the TESLA cavity [17], it was natural to chose the shape of the 2-cell cavity to be TESLA-like for the first iteration (Fig. 37a). However, it turned out that this geometry has a trapped dipole mode. In order to allow this mode to propagate into the beam pipe we decided to use the KEK approach by enlarging one of the beam pipes. We chose the inner radius of one of the beam pipes and the radius of the iris equal to those

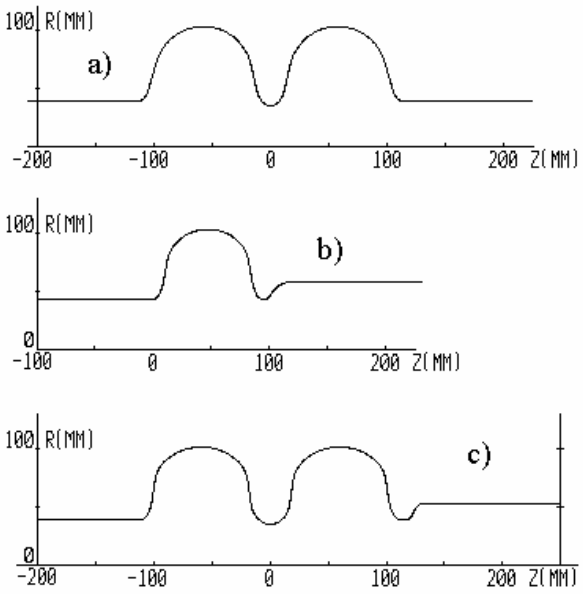

Figure 37: a) Geometry with a trapped dipole mode (TESLA-like); b) KEKB geometry with a propagating dipole mode; c) optimized geometry for the ERL injector with a propagating dipole mode [48].

of TESLA. Scaling of the KEK single-cell dipole-mode-free cavity gave us bigger inner radii. A decrease of the inner iris radius increases the frequency of the dipole mode significantly, so we kept the TESLA value for the inner iris radius. The larger beam pipe, right side in Figs. 37b and 37c, serves for propagating the dipole mode out of the cavity. The right iris (Fig. 37c) secures identity of the fields in both cells but does not preclude the coupling of the dipole mode to the beam pipe.

Having the same frequency as the TESLA cavity [17], it was natural to chose the shape of the 2-cell cavity to be TESLA-like for the first iteration (Fig. 37a). However, it turned out that this geometry has a trapped dipole mode. In order to allow this mode to propagate into the beam pipe we decided to use the KEK approach by enlarging one of the beam pipes. We chose the inner radius of one of the beam pipes and the radius of the iris equal to those of TESLA. Scaling of the KEK single-cell dipole-mode-free cavity gave us bigger inner radii. A decrease of the inner iris radius increases the frequency of the dipole mode significantly, so we kept the TESLA value for the inner iris radius. The larger beam pipe, right side in Figs. 37b and 37c, serves for propagating the dipole mode out of the cavity. The right iris (Fig. 37c) secures identity of the fields in both cells but does not preclude the coupling of the dipole mode to the beam pipe.

The optimization process included taking care not only of the fundamental mode (the surface fields and R/Q), but also of the lowest dipole, TE11-like mode, in which frequency was kept at least 10 MHz above the cut-off frequency of the large beam pipe. Table 3 presents some cavity parameters obtained after the optimization.

The simulation with MultiPac [49] indicate that this cavity shape is free of multipacting. Though the resonant motion of electrons can take place at peak surface electric fields of 30 – 40 MV/m, these fields are well above the operating range and the impact energy of about 26 eV is too low for electron multiplication.

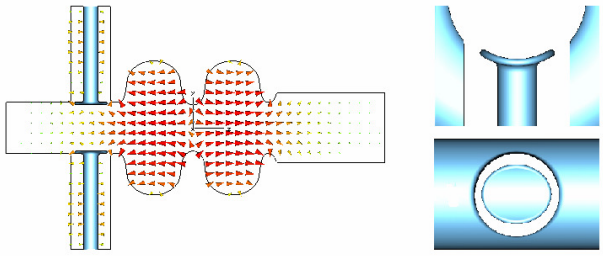

Figure 38: Two-cell cavity with the twin-coaxial input coupler and details of the coupler-cavity interface [50].

Table 3: Selected parameters of the two-cell ERL injector cavity.

frequency	1300 MHz
E_{pk}/E_{acc}	1.94
H_{pk}/E_{acc}	42.8 Oe/(MV/m)
k_c	0.7 %
R/Q	218 Ohm
Q_{ext} **range**	$4.6\times10^4 \ldots 4.1\times10^5$

Input coupler interface optimization

A coaxial coupler was chosen for this cavity. This kind of coupler is easier to make adjustable and it is also simpler to incorporate into the cryomodule. A rather low required external quality factor (see Table 3) may necessitate deep insertion of the antenna into the beam pipe and therefore produce strong transverse kick. This has lead to a twin coupler design [50] (Fig. 38). The on-axis transverse fields from two symmetric couplers cancel each other, thus producing zero kick to beam on axis. Additional benefits are the reduced requirements to per coupler RF power and external Q. The transition from the coaxial line to the beam pipe and the shape of the antenna tip were optimized to get maximal coupling to the cavity.

HOM damping

Sections of the beam pipe lined with microwave-absorbing materials (Fig. 39) are inserted between the cavities to reduce Q factors of higher-order modes. Use of materials with different permeability and permittivity spectra (two types of ferrites and one type of ceramics) allows extending the bandwidth of the load to tens of gigahertz. Unlike the CESR load (Fig. 30), located outside the cryostat at room temperature, the ERL injector load operates inside the cryomodule. The dissipated power is carried out by cold helium gas at a temperature close to 80 K. CLANS simulations of the five-cavity cryomodule equipped with six HOM loads confirmed high efficiency of HOM damping using beam pipe absorbers (Fig. 40).

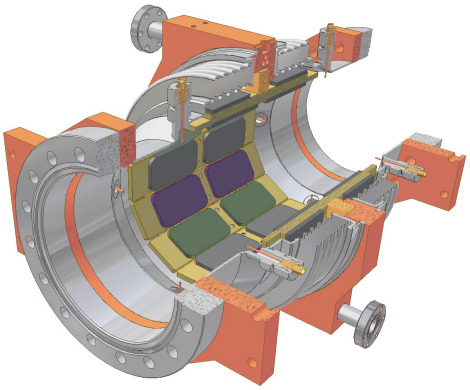

Figure 39: Section view of the Cornell ERL injector ferrite HOM load [51].

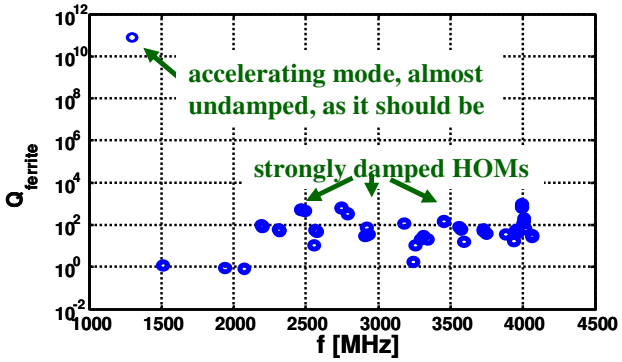

Figure 40: Results of CLANS calculation of HOMs' quality factors for the Cornell ERL injector cryomodule [51].

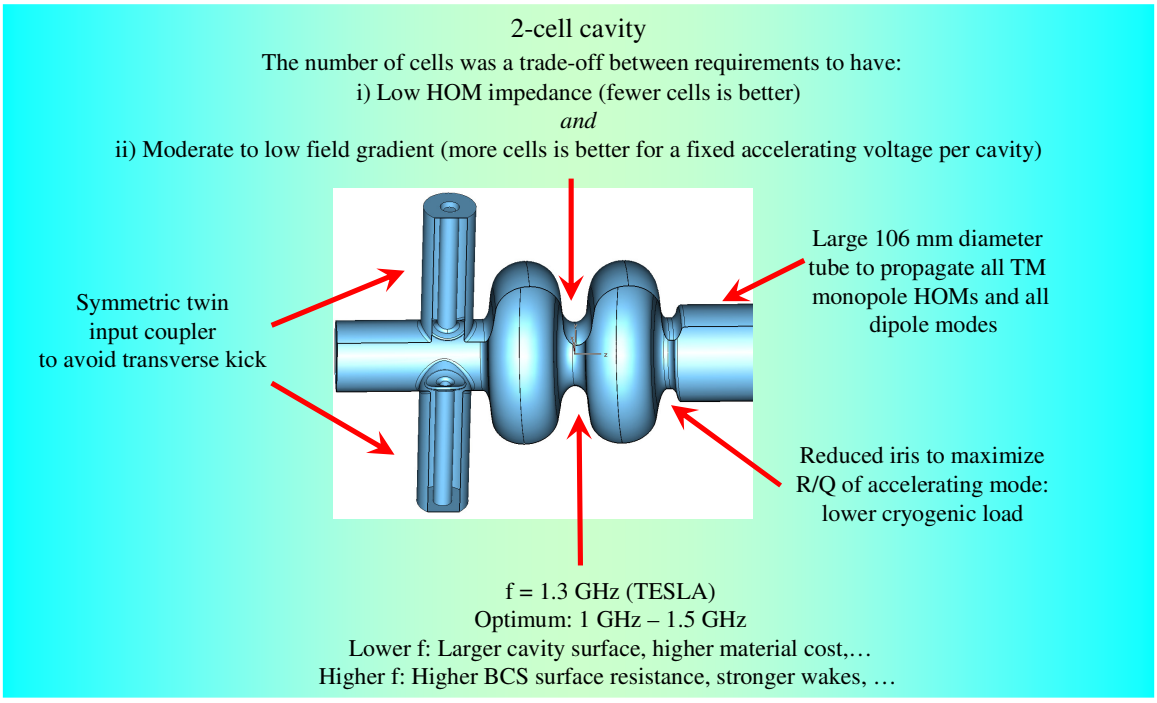

Figure 41: Design features of the two-cell Cornell ERL injector cavity [52].

Highlights of the design

The Cornell ERL injector two-cell cavity illustrates a consistent approach to the design and optimization of a high-β superconducting cavity. Such factors as minimization of the fundamental mode RF losses, taking care of higher-order modes, designing the high average power input coupler with strong coupling and minimal transverse kick were taken into account (Fig. 41).

SUMMARY AND ACKNOWLEDGEMENTS

In this tutorial we discussed different aspects of the high-β superconducting cavity design. Several issues were addressed in detail while others were mentioned only briefly. Choices in cavity design strongly depend on particular accelerator requirements. Therefore a system approach has to be used in designing contemporary superconducting cavities. Modern computer programs and fast computers not only assist in the design process, but allow using multi-variable optimization algorithms. An example of cavity shape optimization was presented. Study of multipacting and beam-cavity interaction must be performed to avoid undesirable effects. Careful attention should be paid to cavity interfaces with other components of a cryomodule. The Cornell ERL injector cavity was used as an example of consistent approach to cavity design.

The authors would like to acknowledge help and advice of H. Padamsee. J. Knobloch kindly provided us his unpublished talk [53].

REFERENCES

[1] H. Padamsee, et al., *RF Superconductivity for Accelerators*, John Wiley & Sons, 1998.

[2] A. Facco, "Low-β Superconducting Cavity Design," these proceedings.

[3] P. Kneisel, et al., "First results on elliptically shaped cavities," *Nucl. Instr. Meth. Phys. Res.*, **188**, 669 (1981).

[4] V. Shemelin, et al., "Optimal cell for TESLA super-conducting structure," *Nucl. Instr. Meth. Phys. Res.*, **A 496**, 1 (2003).

[5] M. M. Karliner, et al., "On the problem of comparison of accelerating structures operated by stored energy," (in Russian), Preprint INP 86-146, Novosibirsk, 1986.

[6] S. Belomestnykh and H. Padamsee, "Performance of the CESR Superconducting RF System and Future Plans," *Proceedings of the 10th Workshop on RF Superconductivity*, Tsukuba, Japan, 2001, pp.197-201.

[7] International Linear Collider, http://www.linearcollider.org/cms/.

[8] K. Floettmann, "The European XFEL Project." this conference.

[9] K. Jordan, et al., "CEBAF Cryomodule Testing," *Proc. of the PAC'91*, San Francisco, CA, v. 4. p. 2381-2383.
P. Kneisel, et al., "Performance of Superconducting Cavities for CEBAF," *Proc. of the PAC'91*, San Francisco, CA, v. 4. p. 2384-2386.

[10] J. Teichert, et al., "RF Status of Superconducting Module Development Suitable for CW Operation: ELBE Cryostat, presented at the ERL'2005 Workshop, Newport News, VA, to be published in *Nucl. Instr. Meth. Phys. Res. A*.

[11] G. Hoffstaetter, et al., "The Cornell ERL Prototype project," *Proc. of the PAC'03*, Portland, OR, pp. 192-194.

[12] R. Calaga, et al., "Ampere Class Linacs: Status Report on the BNL Cryomodule," presented at the ERL'2005 Workshop, Newport News, VA, to be published in *Nucl. Instr. Meth. Phys. Res. A*.

[13] V. Medjidzade, et al., "Design of the CW Cornell ERL Injector Cryomodule," *Proc. of the PAC'05*, Knoxville, TN, pp. 4290-4292.

[14] J. Rathke, et al., "Design and Fabrication of an FEL Injector Cryomodule," *Proc. of the PAC'05,* Knoxville, TN, pp. 3724-3726.

[15] K. Akai, et al., "RF systems for the KEK B-Factory," *Nucl. Instr. Meth. Phys. Res.,* **A 499**, 45 (2003).

[16] D. Boussard and T. Linnecar, "The LHC Superconducting RF System," *Advances in Cryogenic Engineering*, **45**, 385 (1999).

[17] B. Aune, et al., "Superconducting TESLA Cavities," *Phys. Rev. ST AB,* **3**, 092001 (2000).

[18] S. Ramo, J. R. Whinnery, T. Van Duzer, *Fields and Waves in Communication Electronics*, John Wiley & Sons, 1993.

[19] R. Wanzenberg, "Monopole, Dipole and Quadrupole Passbands of the TESLA 9-cell Cavity," Report TESLA 2001-33, September 2001.

[20] Poisson/Superfish, http://laacg.lanl.gov/laacg/services/download_sf.phtml.

[21] D. G. Myakishev, V. P. Yakovlev. "The New Possibilities of SuperLANS Code for Evaluation of Axisymmetric Cavities", *Proc. of the PAC'95*, pp. 2348-2350.

[22] MAFIA, CST GMbH, Buedinger Str. 2a, D-64289, Darmstadt, Germany, http://www.cst.com/Content/Products/MAFIA/Overview.aspx.

[23] CST Microwave Studio, CST GMbH, Buedinger Str. 2a, D-64289, Darmstadt, Germany, http://www.cst.com/Content/Products/MWS/Overview.aspx.

[24] HFSS, Ansoft Corp., http://www.ansoft.com/products/hf/hfss/.

[25] V. Shemelin and S. Belomestnykh, "Calculation of the B-cell Cavity External Q with MAFIA and Microwave Studio," *Proc. of the Workshop on High Power Couplers for SC Accelerators*, Newport News, VA, 2002.

[26] J. Sekutowicz, et al., "Cavities for JLAB's 12 GeV Upgrade," *Proc. of the PAC'2003*, Portland, OR, 2003, pp. 1395-1397.

[27] R. L. Geng et al., "World Record Accelerating Gradient Achieved in a Superconducting Niobium RF Cavity," *Proc. of the PAC'2005*, Knoxville, TN, 2005, pp. 653-655.

[28] R. L. Geng, "Multipacting Simulations for Superconducting Cavities and RF Coupler Waveguides," *Proc. of the PAC'2003*, Portland, OR, 2003, pp. 264-268.

[29] V. Shemelin, "Multipacting in Crossed RF Fields Near Cavity Equator," *Proc. of EPAC'2004*, Lucerne, Switzerland, 2004, pp. 1075-1076.

[30] F. L. Krawczyk, "Status of Multipacting Simulation Capabilities for SCRF Applications," *Proc. of the 10th Workshop on RF Superconductivity*, Tsukuba, Japan, 2001.

[31] Y. H. Chin, "Advances and Applications of ABCI," *Proc. of the PAC'93*, Washington, D.C., v. 2, pp. 3414-3416 (1993).
Y. H. Chin, "User's Guide for ABCI Version 8.8 (Azimutal Beam Cavity Interaction," Report LBL-35258, CERN Preprint SL/94-02 (AP), 1994.

[32] A. Novokhatski, "Code NOVO for wake field calculations," to be published.

[33] P. B. Wilson, "Introduction to Wakefields and Wake Potentials," SLAC-PUB-4547 (1989).

[34] R. Rimmer, et al., "Comparison of Calculated, Measured, and Beam Sampled Impedances of a Higher-Order-Mode-Damped RF Cavity," *Phys. Rev. ST AB*, **3**, 102001 (2000).

[35] R. Rimmer, "Higher-Order Mode Calculations, Predictions and Overview of Damping Schemes for Energy Recovery Linacs," presented at the ERL'2005 Workshop, Newport News, VA, to be published in *Nucl. Instr. Meth. Phys. Res. A*.

[36] E. Haebel, "Wakefields – Resonant Modes and Couplers," *Proc. of the Joint US-CERN-Japan International School "Frontiers of Accelerator Technology"*, Hayama/Tsukuba, Japan, 1996, Eds. S. I. Kurokawa, M. Month and S. Turner, World Scientific, 1999, p. 490.

[37] K. Umemori, et al., "New Higher-order-mode Damping Scheme for L-band Superconducting Cavities Using a Radial Transmission Line," presented at the ERL'2005 Workshop, Newport News, VA, to be published in *Nucl. Instr. Meth. Phys. Res. A*.

[38] S. Belomestnykh, "Review of High Power CW Couplers for Superconducting Cavities," *Proc. of the Workshop on High Power Couplers for SC Accelerators*, Newport News, VA, 2002.

[39] W.-D. Moeller, "High Power Input Couplers for Superconducting Cavities: A Tutorial", these proceedings.

[40] S. Belomestnykh, et al., "Comparison of the Predicted and Measured Loss Factor of the Superconducting Cavity Assembly for the CESR Upgrade," Proc. of the PAC'95, Dallas, TX, pp. 3394-3396.

[41] J. R. Delayen, et al., "An R.F. Input Coupler System for the CEBAF Energy Upgrade Cryomodule," *Proc. of the PAC'99,* New York, NY, pp. 1462-1464.

[42] J. R. Delayen, et al., "Cryomodule Development for the CEBAF Upgrade," *Proc. of the PAC'99,* New York, NY, pp. 934-936.
E. Daley, et al., "Improved Prototype Cryomodule for the CEBAF 12 GeV Upgrade," *Proc. of the PAC'03*, Portland, OR, pp. 1377-1379.

[43] E. N. Schmierer, et al., "Results of the APT RF Power Coupler Development for Superconducting Linacs," *Proc. of the 10th Workshop on RF Superconductivity*, Tsukuba, Japan, September 2001.

[44] ANSYS, http://www.ansys.com/

[45] D. Proch, "Superconducting Cavities for $v_p = c$ Linacs, Storage Rings, & Synchrotrons," in *Handbook of Accelerator Physics and Engineering*, World Scientific, 2002, p. 530.

[46] M. Liepe, et al., "Dynamic Lorentz Force Compensation with a Fast Piezoelectric Tuner," *Proc. of the 10th Workshop on RF Superconductivity*, Tsukuba, Japan, 2001.

[47] J. R. Delayen, "Ponderomotive Instabilities and Microphonics – a Tutorial," this conference.

[48] V. Shemelin, et al., "Dipole-Mode-Free and Kick-Free 2-Cell Cavity for the SC ERL Injector," *Proc. of the PAC'2003*, Portland, OR, 2003, pp. 2059-2061.

[49] P. Ylä-Oijala, et al., "MultiPac – Multipacting Simulation Package with 2D FEM Field Solver," *Proc. of the 10th Workshop on RF Superconductivity*, Tsukuba, Japan, 2001.

[50] V. Shemelin, S. Belomestnykh, H. Padamsee, "Low-kick Twin-coaxial and Waveguide-coaxial Couplers for ERL", Cornell LEPP Report SRF 021028-08 (November 28, 2002).

[51] M. Liepe, et al., "Broadband HOM Absorber for the Cornell ERL," these proceedings.

[52] The idea of this illustration is due to M. Liepe (Cornell University).

[53] J. Knobloch, "Tutorial: RF-Cavity Design for High-Current Storage Rings" talk delivered at the 11th Workshop on RF Superconductivity (September 2003, Luebeck/Travemuende, Germany), unpublished.